

# Estimation of the skull insertion loss using an optoacoustic point source

Héctor Estrada<sup>a</sup>, Johannes Rebling<sup>a,b</sup>, Jake Turner<sup>a,b</sup>, Moritz Kneipp<sup>a,b</sup>, Shy Shoham<sup>c</sup>, and Daniel Razansky<sup>a,b</sup>

<sup>a</sup>Institute for Biological and Medical Imaging (IBMI), Helmholtz Zentrum München, Germany

<sup>b</sup>School of Medicine and School of Electrical Engineering and Information Technology, Technical University of Munich, Germany

<sup>c</sup>Department of Biomedical Engineering, Technion Israel Institute of Technology, Haifa, Israel

## ABSTRACT

The acoustically-mismatched skull bone poses significant challenges for the application of ultrasonic and optical techniques in neuroimaging, still typically requiring invasive approaches using craniotomy or skull thinning. Optoacoustic imaging partially circumvents the acoustic distortions due to the skull because the induced wave is transmitted only once as opposed to the round trip in pulse-echo ultrasonography. To this end, the mouse brain has been successfully imaged transcranially by optoacoustic scanning microscopy. Yet, the skull may adversely affect the lateral and axial resolution of transcranial brain images. In order to accurately characterize the complex behavior of the optoacoustic signal as it traverses through the skull, one needs to consider the ultrawideband nature of the optoacoustic signals.

Here the insertion loss of murine skull has been measured by means of a hybrid optoacoustic-ultrasound scanning microscope having a spherically focused PVDF transducer and pulsed laser excitation at 532 nm of a 20  $\mu\text{m}$  diameter absorbing microsphere acting as an optoacoustic point source. Accurate modeling of the acoustic transmission through the skull is further performed using a Fourier-domain expansion of a solid-plate model, based on the simultaneously acquired pulse-echo ultrasound image providing precise information about the skull's position and its orientation relative to the optoacoustic source. Good qualitative agreement has been found between the a solid-plate model and experimental measurements.

The presented strategy might pave the way for modeling skull effects and deriving efficient correction schemes to account for acoustic distortions introduced by an adult murine skull, thus improving the spatial resolution, effective penetration depth and overall image quality of transcranial optoacoustic brain microscopy.

**Keywords:** optoacoustic microscopy, photoacoustic microscopy, mouse skull modeling, neuroimaging, transcranial brain imaging, mouse skull insertion loss

## 1. INTRODUCTION

Optoacoustic neuroimaging is attracting considerable attention due to its potential for imaging deep structures with molecular contrast.<sup>1</sup> As a hybrid technique, optoacoustic imaging shares advantages of optical and ultrasound imaging. The skull is, however, an obstacle for ultrasound propagation. So far only applications involving one-way ultrasound transmission through the skull have been proven successful such as optoacoustic neuroimaging,<sup>2</sup> ultrasound neurostimulation,<sup>3</sup> blood brain barrier opening for drug delivery,<sup>4</sup> and transcranial focused ultrasound surgery.<sup>5</sup> These applications require accurate information of acoustic properties of the skull to attain high resolution at a given depth. The ultrasound wave is distorted due to the solid nature of the skull, its curvature and inhomogeneities. Depending on the thickness to wavelength ratio  $h/\lambda$  the distortion can be more ( $h/\lambda \gg 1$ ) or less ( $h/\lambda \leq 1$ ) severe.

Measuring the acoustical properties of the skull is not trivial. Particularly in the case of mice, traditional methods used in nondestructive testing of plates<sup>6</sup> are not suitable due to size constraints.

Further author information: (Send correspondence to D.R.)  
D.R.: E-mail: dr@tum.de

Photons Plus Ultrasound: Imaging and Sensing 2016, edited by Alexander A. Oraevsky, Lihong V. Wang  
Proc. of SPIE Vol. 9708, 97080M · © 2016 SPIE · CCC code: 1605-7422/16/\$18 · doi: 10.1117/12.2211183

Here we propose a skull characterization technique for dual optoacoustic-ultrasound microscopy with a single scanning focused detector and using an optoacoustic point source.

## 2. INSERTION LOSS MEASUREMENT

The basis of our experimental setup is the dual optoacoustic-ultrasound scanning microscope described in.<sup>7</sup> Figure 1 shows the geometry of our technique as well as the experimental setup.

A single black polyethylene sphere of 20  $\mu\text{m}$  in diameter (Cospheric LLC, Santa Barbara, USA) is fixed in a clean agarose block and placed in a small tray filled with phosphate-buffered saline solution (Life Technologies Corp., UK) as the immersion liquid. Next to the microsphere and without interfering the acoustic path, a multimode optical fiber (MMF) delivers the light generated by a Q-switched diode end pumped Nd:YAG laser (Model: IS8II-E; EdgeWave GmbH, Würselen, Germany). In our experiments we used light pulses of 10 ns in width, 532 nm in wavelength, and with an energy between 100 - 500  $\mu\text{J}$ . In order to avoid distortions in the light propagation due to the presence of the skull and minimize the generation of parasitic signals, the illumination to excite the microsphere is placed below the skull and perpendicular to the transducer as depicted in Fig. 1.

The spherically focused Polyvinylidene Fluoride (PVdF) ultrasound transducer (Precision Acoustics, Dorchester, United Kingdom) with a focal distance of 6.6 mm, an active diameter of 6 mm, and a -6 dB bandwidth ranging from 10 MHz to 40 MHz is scanned in pulse-echo mode over the agar block to find the microsphere guided by indentations made in the agar surface. Once the sphere is found, the direct optoacoustic signal generated by the microsphere  $s(t)$  is recorded. Next, a piece of the right parietal mouse skull (17 weeks old Athymic nude Foxn1<sup>nu</sup> mouse, Harlan, The Netherlands) is positioned between the microsphere and the transducer. Then, the signal with the skull obstructing the propagation path  $s'(t)$  is acquired and the skull insertion loss can be calculated after transforming the signals to the frequency domain as  $\text{IL}(\omega) = 20 \log(S(\omega)/S'(\omega))$ .

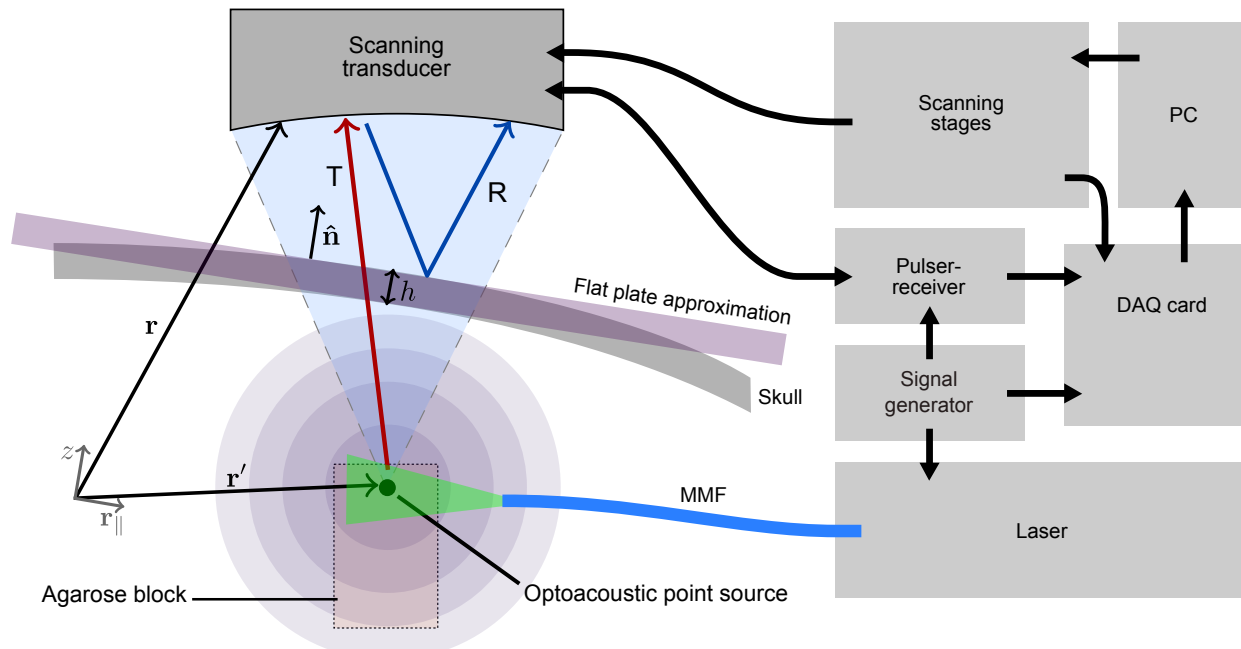


Figure 1. Schematic showing the geometry of the technique and the experimental setup. T denotes the wave transmitted from the source to the detector through the skull and R the wave reflected in pulse-echo mode

As a next step a pulse-echo scan of the skull is performed to extract the position and orientation using cross correlation. It is important to scan a region that is bigger than the projection of the transducer's acceptance cone on the skull (PTACS) to ensure accurate results. The source-skull distance and the skull normal vector  $\hat{\mathbf{n}}$  (see Fig. 1) are calculated by fitting a plane to the PTACS.

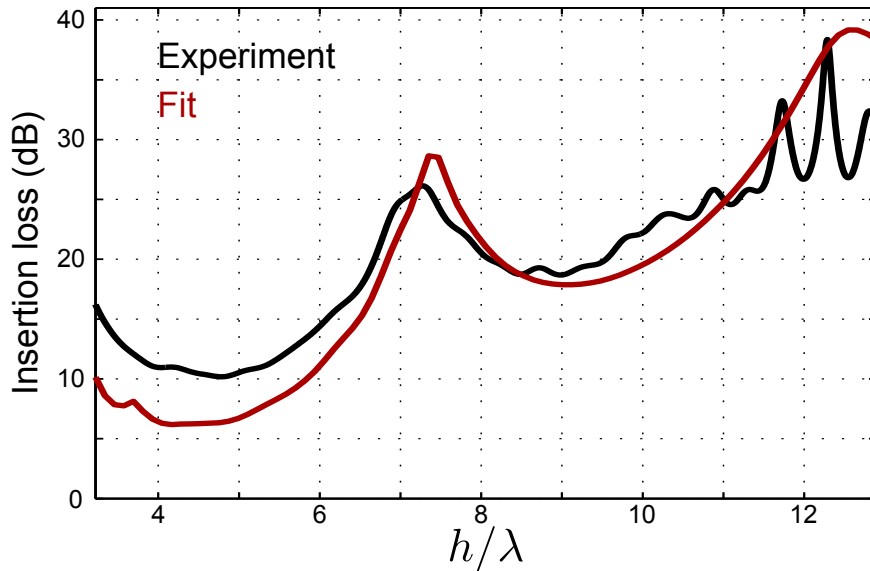


Figure 2. Measured skull insertion loss and theoretical model fit as a function of the thickness to wavelength-in-the-fluid ratio  $h/\lambda$

### 3. SKULL MODEL AND FIT

A simple, yet rigorous, skull model is developed to fit the experimental curve and hence extract the elastic constants that characterize the skull. A detailed description of the model and the fitting procedure can be found in.<sup>8</sup> Provided that the PTACS is small enough, the skull surface can be considered as a flat solid plate (see Fig. 1). For simplicity, we model the skull as an homogeneous isotropic viscoelastic solid fully characterized by these 6 parameters: the thickness  $h$ , the density  $\rho$ , the longitudinal speed of sound  $c_\ell$ , the transverse speed of sound  $c_t$  and the viscoelastic losses  $\chi, \eta$ .<sup>9</sup> In the fluid, we use the angular spectrum method to describe the point source and forward propagate the acoustic wave up to the detector surface. The effect of the skull enters via multiplication by its transmission amplitude in reciprocal and frequency domain. A genetic algorithm<sup>8</sup> is used to fit the model to the experimental curve. For the immersion fluid we assumed  $c = 1505$  (m/s), and  $\rho = 1000$  (kg/m<sup>3</sup>).

### 4. RESULTS

A comparison between the measured and the fitted skull insertion loss is shown in Fig. 2 as a function of the thickness to wavelength ratio  $h/\lambda$ . The general trend of the insertion loss is well represented by the model, although there are significant differences at  $h/\lambda \sim 4$  and  $h/\lambda \sim 12$ . The parameters retrieved from the fit are  $h = 458 \mu\text{m}$ ,  $\rho = 1969 \text{ kg/m}^3$ ,  $c_\ell = 2242 \text{ m/s}$ ,  $c_t = 1710 \text{ m/s}$ ,  $\chi = 0.79 \text{ Pa}\cdot\text{s}$ , and  $\eta = 1.99 \text{ Pa}\cdot\text{s}$ .<sup>8</sup> As can be seen from the insertion loss curve, the effect of a  $458 \mu\text{m}$  skull between 10 and 40 MHz is considerably high and non-monotonic. The optoacoustic signals acquired transcranially from the mouse brain through such a skull would thus suffer a strong filtering of its high frequency components. The signal degradation equally affects optical resolution or acoustic resolution optoacoustic techniques as demonstrated in.<sup>10</sup>

### 5. CONCLUSIONS

We developed a method for the measurement of the skull's insertion loss. In addition, coregistered pulse-echo ultrasound data allows us to fit a skull model which returns the skull elastic constants for the region within the transducer's acceptance cone.

The insertion loss obtained by this method depends strongly on the detector's geometry and its relative position to the skull, whereas the estimated parameters are universal within the homogeneous skull model. One

of the main advantages of the method is the simplicity of the coregistration between optoacoustic and pulse-echo ultrasound, which is performed by the same transducer. No additional imaging techniques such as X-ray computed tomography are required. Both the model and the measurement technique are flexible and do not require the skull to be perfectly perpendicular to the transducer axis.

The insertion loss of a mouse skull of  $\sim 450 \mu\text{m}$  shows a maximum of 40 dB beyond 40 MHz and a non monotonic behavior. Full transmission windows reported previously<sup>10</sup> for a  $230 \mu\text{m}$  thick mouse skull were not visible due to the difference in skull thickness and the frequency range used.

Our theoretical framework is flexible and more realistic skull model could be easily used. We hope this work paves the way towards a better understanding of the acoustic properties of the skull and eventually leads to skull distortion correction.

## ACKNOWLEDGMENTS

This project was supported in part by the European Research Council through the grant agreement ERC-2010-StG-260991. D. R. and J. R. acknowledge support from the European Research Council through the Initial Training Network Grant Nr. 317526. We gratefully acknowledge Ali Özbek for the useful discussions.

## REFERENCES

- [1] Ntziachristos, V., “Going deeper than microscopy: the optical imaging frontier in biology,” *Nat Meth* **7**, 603–614 (Aug. 2010).
- [2] Yao, J. and Wang, L. V., “Photoacoustic brain imaging: from microscopic to macroscopic scales,” *Neurophotonics* **1**(1), 011003 (2014).
- [3] Tufail, Y., Matyushov, A., Baldwin, N., Tauchmann, M. L., Georges, J., Yoshihiro, A., Tillery, S. I. H., and Tyler, W. J., “Transcranial pulsed ultrasound stimulates intact brain circuits,” *Neuron* **66**(5), 681 – 694 (2010).
- [4] Aryal, M., Arvanitis, C. D., Alexander, P. M., and McDannold, N., “Ultrasound-mediated blood-brain barrier disruption for targeted drug delivery in the central nervous system,” *Advanced Drug Delivery Reviews* **72**, 94 – 109 (2014). Ultrasound triggered drug delivery.
- [5] Coluccia, D., Fandino, J., Schwyzer, L., O’Gorman, R., Remonda, L., Anon, J., Martin, E., and Werner, B., “First noninvasive thermal ablation of a brain tumor with mr-guided focused ultrasound,” *Journal of Therapeutic Ultrasound* **2**, 17 (2014).
- [6] Fei, D., Chimenti, D. E., and Teles, S. V., “Material property estimation in thin plates using focused, synthetic-aperture acoustic beams,” *J. Acoust. Soc. Am.* **113**(5), 2599–2610 (2003).
- [7] Estrada, H., Sobol, E., Baum, O., and Razansky, D., “Hybrid optoacoustic and ultrasound biomicroscopy monitors laser-induced tissue modifications and magnetite nanoparticle impregnation,” *Laser Physics Letters* **11**(12), 125601 (2014).
- [8] Estrada, H., Rebling, J., Turner, J., and Razansky, D., “Broadband acoustic properties of a murine skull,” *under review* (2015).
- [9] Brekhovskikh, L. M. and Godin, O. A., [*Acoustics of Layered Media*], vol. I of *Springer Series on Wave Phenomena*, Springer-Verlag Berlin Heidelberg New York, 2nd ed. (1998).
- [10] Kneipp, M., Turner, J., Estrada, H., Rebling, J., Shoham, S., and Razansky, D., “Effects of the murine skull in optoacoustic brain microscopy,” *Journal of Biophotonics* **9**(1-2), 117–123 (2016).